Solar hydrogen production with cerium oxides thermochemical cycle

Marco Binotti, Gioele Di Marcoberardino, Mauro Biassoni, and Giampaolo Manzolini

Citation: AIP Conference Proceedings **1850**, 100002 (2017); doi: 10.1063/1.4984459
View online: http://dx.doi.org/10.1063/1.4984459
View Table of Contents: http://aip.scitation.org/toc/apc/1850/1
Published by the American Institute of Physics

Solar Hydrogen Production with Cerium Oxides Thermochemical Cycle

Marco Binotti[1, a)], Gioele Di Marcoberardino, Mauro Biassoni, Giampaolo Manzolini

[1]*Politecnico di Milano, Dipartimento di Energia, via Lambruschini 4, 20156 Milano, Italy*

[a)]Corresponding author: marco.binotti@polimi.it

Abstract. This paper discusses the hydrogen production using a solar driven thermochemical cycle. The thermochemical cycle is based on nonstoichiometric cerium oxides redox and the solar concentration system is a solar dish. Detailed optical and redox models were developed to optimize the hydrogen production performance as function of several design parameters (i.e. concentration ratio, reactor pressures and temperatures) The efficiency of the considered technology is compared against two commercially available technologies namely PV + electrolyzer and Dish Stirling + electrolyzer. Results show that solar-to-fuel efficiency of 21.2% can be achieved at design condition assuming a concentration ratio around 5000, reduction and oxidation temperatures of 1500°C and 1275 °C. When moving to annual performance, the annual yield of the considered approach can be as high as 16.7% which is about 43% higher than the best competitive technology. The higher performance implies that higher installation costs around 40% can be accepted for the innovative concept to achieve the same cost of hydrogen.

INTRODUCTION

The major drivers that boost the development of hydrogen as energy carrier are: i) energy security supply (hydrogen can be produced by different sources), ii) urban air quality improvement and iii) integration with non-dispatchable renewables to store energy compensating their randomness.

Currently the world hydrogen production, about 600-720 Billions of Nm^3/y, comes mainly from fossil fuels via natural gas steam reforming (50%), oil/naptha reforming (30%) and coal gasification (30%); the remaining 4% is mainly produced with water electrolysis. In order to have a sustainable and near zero emission hydrogen economy, it is crucial to decarbonize the hydrogen production relying on renewable energy sources (RES). Nowadays, the key technology for the so-called "Green Hydrogen" production (i.e. hydrogen produced with RES) is electrochemical water splitting with green electricity produced by PV or wind turbines, although in the "Study on Hydrogen from renewable resources in the EU", recently presented by the FCH-JU [1], alternative pathways for green hydrogen production have been identified. Among these paths, CSP coupled with thermochemical cycles for water splitting is seen as a promising option with a Technology Readiness Level (TRL) of 5, expected to grow to 7 within 2030.

The use of solar energy as heat input for thermochemical cycles was considered for the first time at the beginning of the XXI century, abreast of the improvement of concentration ratio (CR) [2]. Among the numerous analyzed cycles [3,4], the most investigated ones, both from an experimental and from the reactor design point of view, are based on sulfur [3,5,6], iron [7–9], zinc [8,10,11] and cerium [10,12,13]. Typically, thermochemical cycles require high operating temperature making point focus systems (solar tower and solar dish) as the most suitable solution because of the high concentration ratios.

In the present work, the nonstoichiometric configuration of cerium oxide thermodynamic cycle combined with parabolic dish is investigated. The advantages of cerium oxide are the absence of corrosion effects (sulfur) and fast sintering (iron), low recombination after the reactions (zinc), solid state during all the cycle, rapid kinetics and the possibility to use solid-solid heat recovery [14,4,12].

SolarPACES 2016
AIP Conf. Proc. 1850, 100002-1–100002-10; doi: 10.1063/1.4984459
Published by AIP Publishing. 978-0-7354-1522-5/$30.00

Results in terms of solar-to-fuel conversion efficiency at design condition, yearly hydrogen yield and preliminary economic assessment are determined and compared against the efficiencies obtainable with an electrolyzer coupled either with a dish Stirling engine or with a PV system.

METHODOLOGY

Different models were developed to simulate the different conversion processes occurring in the solar thermochemical plant: in particular, the thermochemical reactor model suggested by [15] was implemented in an Excel spreadsheet, while the optical performance of the solar dish and of the secondary receiver were carried out with SolTrace [16] (see Figure 1). The two models (concentrator and reactor) were assembled in order to determine the effects of the secondary reflector type (CPC or V-trough), acceptance angle (θ_a) and position on the reactor performance at different operating conditions (p_{ox}, p_{red}, T_{ox}, T_{red}). The selected optimum configuration is the best compromise between dish+secondary reflector optical performance (η_{opt}) and reactor performance ($\eta_{reactor}$), leading to the highest hydrogen production and thus to the solar-to-fuel efficiency defined as:

$$\eta_{solar-to-fuel} = \eta_{opt} \times \eta_{reactor} = \frac{\dot{Q}_{abs,react}}{DNI \times A_{dish}} \times \frac{\dot{n}_{H_2} HHV_{H_2}}{\dot{Q}_{abs,react}} = \frac{\dot{n}_{H_2} HHV_{H_2}}{\dot{Q}_{sun}} \quad (1)$$

where A_{dish} is the parabolic dish aperture area, DNI is the direct normal irradiance, $\dot{Q}_{abs,react}$ is the radiation absorbed by the reactor window and $\dot{n}_{H_2}$ is the molar flow of hydrogen multiplied by its higher heating value (HHV_{H_2}).

The off-design behavior of the optimized system as function of the DNI was computed assuming for simplicity a constant reactor temperature as well as thermal losses. For two different sites (Las Vegas and Sevilla), the performance of the system in terms of yearly hydrogen yield (YHY, kg_{H2}/y) were compared against two alternative solar driven hydrogen production systems:

- a parabolic dish with Stirling engine coupled with an alkaline electrolyzer;
- a PV system with the same aperture area ($A_{PV}=A_{dish}$) coupled with an electrolyzer.

The selected dish/Stirling system is similar to the EuroDish SBP system, located at the "Plataforma Solar de Almeria" [17], that uses a SOLO 161V1 engine of 10 kW_e and whose main characteristics are reported in Table 1. The photovoltaic system uses LG Electronics LG250S1K–A3 monocrystalline Si modules [18] [19] mounted with an optimized tilt angle β; the main PV characteristics are also reported in Table 1.

The electric power produced by the two alternative driven solar systems is then converted into hydrogen with an alkaline electrolyzer. Nowadays there are three commercially available types of electrolyzer: alkaline, PEM (Proton Exchange Membrane) and AEM (Anion Exchange Membrane) [20]. In these simulations the alkaline electrolyzer was chosen because it has the lowest cost and average performances; moreover, alcakaline electrolizer can be used at any plant size, unlike PEM and AEM that are limited. The efficiency of the electrolyzer was taken equal to 52 kWh_{el}/kg_{H2}**,** constant in the analyzed operating conditions [20].

TABLE 1. Main information about dish/stirling system [17], PV system [18] and electrolyzer [20]

Dish/Stirling System (EuroDish SBP)		**Photovoltaic System (LG Electronics LG250S1K–A3)**		**Electrolyzer**	
Dish Aperture Area, (m^2)	56.7	Panel aperture area (m^2)	1.59	Size (Nm^3_{H2}/h)	0.25 – 760
Aperture Diameter (m)	0.15	Panel max power (W)	250.4	Size (kW)	1.8 – 5300
Intercept factor (-)	0.93	Panel max voltage (V)	30.8	H_2 purity (%)	99.5-99.9998
Stirling size (kW)	10	Panel max current (A)	8.1	Efficiency(kWh_{el}/kg_{H2})	52
Nominal efficiency (%)	19	Nominal Efficiency (%)	15.8		

The two alternative systems off-design performance and yearly productivities were computed with the System Advisor Model (SAM) [19]. Finally, the Levelized Cost of produced Hydrogen (LCOH) was computed for the two alternative systems and the investment cost of the thermochemical reactor was chosen in order to match the same LCOH, defined as:

$$\text{LCOH}\left[\frac{€}{kWh_{H_2}}\right] = \frac{C_{INV} \times FCR}{\dot{n}_{H_2,y} \times HHV_{H_2}} + \frac{C_{O\&M}}{\dot{n}_{H_2,y} \times HHV_{H_2}} \quad (2)$$

The Fix-charge Rate (*FCR*) method [21] allows distributing the investment cost (C_{INV}) over the total plant lifetime: *FCR* is defined as the fraction of the total cost that the investor has to cover every year to face yearly depreciation or return of the capital, tax and insurance expenses associated with the installation of a particular generating unit. FCR was assumed equal to 10.05%.

A schematic of the adopted methodology is summarized in Figure 1.

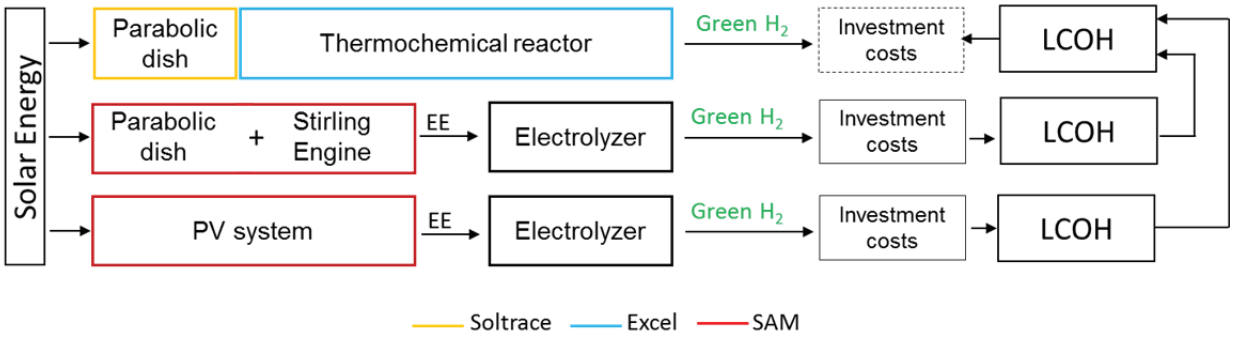

FIGURE 1. Methodology adopted to determine the LCOH of the alternative technologies and the reactor investment cost.

THERMOCHEMICAL SYSTEM DESIGN AND PERFORMANCE

Thermochemical Reactor

The thermochemical reactor model based on the work of Bader et al. [15] and implemented in Excel aims at predicting the hydrogen production and solving the system mass/energy balance as function of the operating conditions (T,p) for a given heat input. The reactor is divided into two parts in which endothermic reduction of cerium oxide (1) and its exothermic oxidation (2) occur. The two reactions are reported below:

$$\frac{1}{\Delta\delta}\text{CeO}_{2-\delta_{ox}} \rightarrow \frac{1}{\Delta\delta}\text{CeO}_{2-\delta_{red}} + \frac{1}{2}\text{O}_2 \quad (3)$$

$$\frac{1}{\Delta\delta}\text{CeO}_{2-\delta_{red}} + \text{H}_2\text{O} \rightarrow \frac{1}{\Delta\delta}\text{CeO}_{2-\delta_{ox}} + \text{H}_2 \quad (4)$$

$\Delta\delta = \delta_{red} - \delta_{ox}$ represents the oxygen variation in the cerium oxide stoichiometry with the value of δ as function of temperature (up to 1500°C) and oxygen partial pressure taken from the experimental studies of Panlener [22] and Ricken et al. [23]. The trend of $-\log(\delta)$ is reported in Figure 2a. On the reduction side a sweep gas (N_2) is used to take out the oxygen, while on the oxidation side steam is introduced and, after oxidation, a mixture of steam and hydrogen with small traces of oxygen is obtained. The model schematic is reported in Figure 2b.

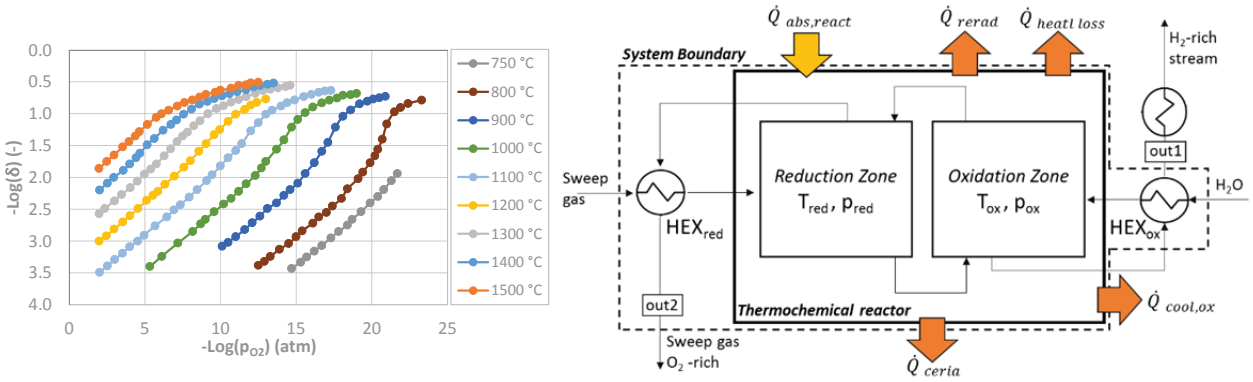

(a) (b)

FIGURE 2: (a) δ as function of temperature and oxygen partial pressure (adapted from [22]) and (b) schematic of the studied reactor adapted from [15].

In the present study, only the thermodynamic aspects of the reactor were considered, while the technological challenges related to its realization were not deepened: it was thus assumed the possibility of having different temperatures (T_{ox}, T_{red}) and pressures (p_{ox}, p_{red}) for the two reactor zones; also the possibility of a heat recovery system between oxidized and reduced cerium was also investigated in case of non-isothermal reactor ($T_{ox} \neq T_{red}$). The efficiency of recovery between oxidized and reduced cerium oxide (η_{ceria}) was initially set equal to zero. Two recuperative heat exchangers (HEX_{ox}/HEX_{red}) and a further heat exchanger to condensate steam allowing for hydrogen separation were also considered in the system. Thermodynamic properties of gas/steam mixtures were computed using FluidProp [24], while cerium oxide specific heat as function of its oxidization state was taken from [25].

The model allows solving all the energy and mass balances assuming chemical equilibrium compositions in all the thermodynamic points of the system. The energy balance of the reactor is:

$$\dot{Q}_{abs,react} - \dot{Q}_{rerad} - \dot{Q}_{heat\ loss} + \dot{Q}_{chem,red} - \dot{Q}_{gases,red} + \dot{Q}_{chem,ox} - \dot{Q}_{gases,ox} - \dot{Q}_{cool,ox} - \dot{Q}_{ceria} = 0 \qquad (5)$$

where $\dot{Q}_{abs,react}$ is the reactor heat input, $\dot{Q}_{chem,red}$ and $\dot{Q}_{chem,ox}$ are the heat absorbed/released by the reactions on the reduction/oxidation zones, $\dot{Q}_{gases,red}$ and $\dot{Q}_{gases,ox}$ are the heat required to rise the temperatures of reactants up to the corresponding reactor zone temperature (T_{red} and T_{ox} respectively), $\dot{Q}_{cool,ox}$ is a further heat rejection needed if the heat released in the oxidation zone $\dot{Q}_{chem,ox}$ is larger than $\dot{Q}_{gases,ox}$, $\dot{Q}_{ceria}$ takes into account the heat required to heat up cerium oxide from oxidation to reduction temperature ($\dot{Q}_{ceria} = 0$ for an isothermal reactor) and finally $\dot{Q}_{rerad}$ and $\dot{Q}_{heat\ loss}$ take into account radiation and convection losses respectively. The heat released by radiation $\dot{Q}_{rerad}$ is proportional to the reactor aperture area $\dot{Q}_{rerad} = A_{aperture}\sigma T_{red}^4$ and thus is related to the concentration ratio of the optical system. The main assumptions used in the model are reported in Table 2.

TABLE 2. Main input data for the reactor model.

Thermochemical reactor	
Maximum reduction zone temperature, $T_{red,MAX}$ (°C)	1500
Fraction of oxygen at reduction zone inlet, $x_{O2,in}$ (-)	10^{-6}
HEX_{red}/HEX_{ox} effectiveness, $\varepsilon_{red}/\varepsilon_{ox}$	0.96/0.6
Cerium heat recovery efficiency, η_{ceria}	0
Thermal losses factor, F (-)	0.2

Results were validated against data given in [15], showing good agreement. Several parametric analyses were conducted in order to test the effect of the operating conditions variation on the reactor efficiency (defined as hydrogen production divided by the reactor heat input). In Figure 3a the effect of the variation of the system temperature for an isobaric, isothermal reactor on the system molar flows is reported, showing how the temperature increase is crucial for a higher hydrogen yield. In Figure 3b, both the effects of system pressure and of a differential

temperature between oxidation and reduction zone are assessed, showing a beneficial effect with the reduction of the system pressure that increases the value of Δδ. The best efficiency for an isobaric reactor, around 40%, is obtained with a ΔT of about 75°C operating at sub-atmospheric pressure as low as 0.01 atm; further analyses showed a potential 3 points percent solar-to-fuel efficiency increase if the oxidization zone is kept at higher pressures with respect to the reduction zone (p_{red}=0.01bar and p_{ox}=10bar).

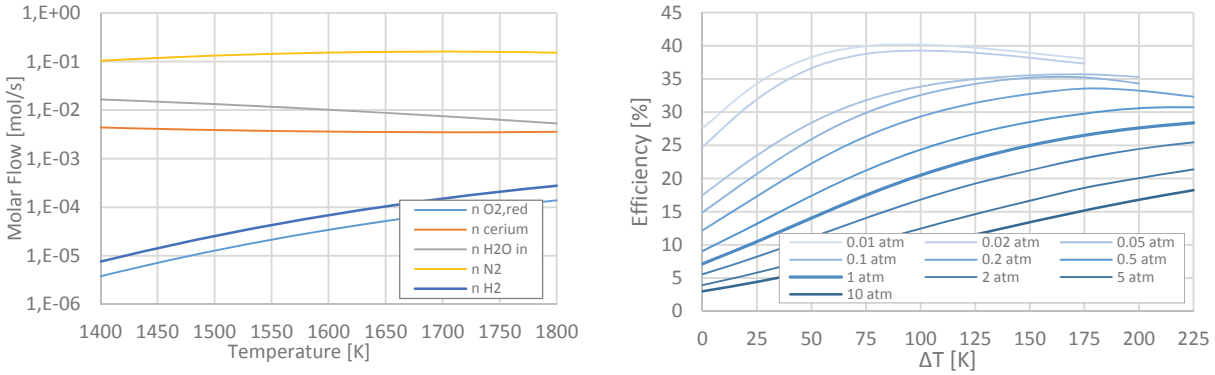

(a) (b)

FIGURE 3: (a) Molar flows of the main reactor streams as function of the system operating temperature and (b) reactor efficiency as function of the system pressure (p_{red}=p_{ox}) and of the ΔT between reduction and oxidation zones (T_{red}=$T_{red,max}$). In both cases $\dot{Q}_{abs,react}$ is assumed equal to 42.3 kW

For the coupling with the solar system an atmospheric reactor was selected, in order to avoid complex management related to subatmospheric operation. In order to maximize the reactor efficiency, a maximum ΔT of 225 K between reduction and oxidation zones was chosen, allowing to reach about 28% of reactor efficiency.

Concentration System

The high temperatures of the thermochemical reactor require a high concentration ratio (>3000): therefore, a parabolic dish coupled with a secondary reflector is designed and its optical performance are estimated with SolTrace. The selected parabolic mirror is the one used in the SBP EuroDish system [17], while the chemical reactor is supposed to have a circular quartz window of radius *r* with a secondary reflector CPC or V-trough shaped. The need for a secondary reflector is strictly related to the slope errors of the primary mirrors: for a given radius *r* there is a value of slope below which no secondary mirror is needed. The main input for the optical simulation are reported in Table 3.

TABLE 3. Main input data for the optical model.

Parabolic Dish	
Dish Aperture Area (m^2), A_{dish}	56.7
Mirror reflectivity (-)	0.94
Nominal DNI, G_0 (W/m^2)	1000
Mirror specularity errors σ_M (mrad)	0.2
Mirror slope errors σ_S (mrad)	2.5
Quartz refraction index, *n*	1.4585

Figure 4a reports a screenshot of the SolTrace model, while Figure 4b shows the optical efficiency trend for a receiver with $r = 6cm$, for different secondary reflector shape as function of the slope error. Assuming a slope error of 2.5 mrad the best secondary was selected: a CPC type with an acceptance angle of 50.5° that guarantees an overall optical efficiency of about 75%. With respect to 56.7 kW of solar power hitting the dish, only 42.3 kW are absorbed by the reactor, due to the losses related to the dish reflectivity ($\dot{Q}_{dish,loss} = 3.8\,kW$) and to the CPC reflectivity, intercept factor and quartz window reflectivity ($\dot{Q}_{CPC,loss} = 10.8\,kW$).

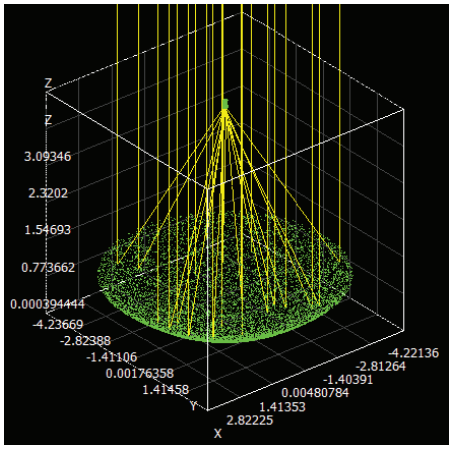

(a)

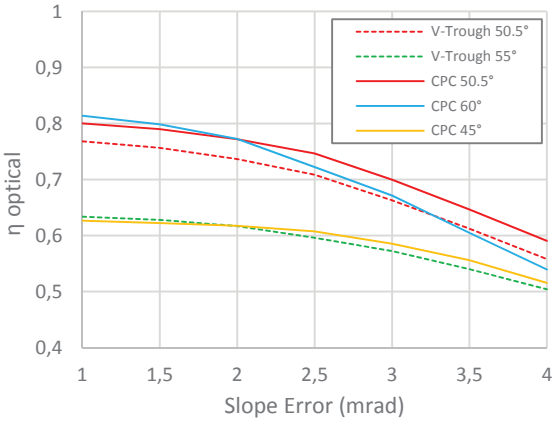

(b)

FIGURE 4: (a) Screenshot of the SolTrace simulation of the parabolic dish and of the secondary reflector and (b) optical efficiency for different receiver shapes as function of the slope error ($r = 6cm$).

Overall System Nominal Performance

The concentration system and the thermochemical reactor models were combined in order to obtain the overall solar-to-fuel efficiency. In Figure 5a, the effect of the CR on the $\eta_{Solar\text{-}to\text{-}fuel}$ for the selected solar-thermochemical system is reported, showing a maximum of 21.2% for an absorber radius of 6 cm, which corresponds to a geometric CR of 5017; this case was thus selected as design condition and for the subsequent yearly analysis. The overall energy balance, reported in Figure 5b for the design case, can be written as:

$$\dot{Q}_{sun} - \dot{Q}_{dish,loss} - \dot{Q}_{CPC,loss} - \dot{Q}_{rerad} - \dot{Q}_{heat\ loss} - \dot{Q}_{out2} - \dot{Q}_{out1} - \dot{Q}_{cool,ox} - \dot{Q}_{ceria} = \dot{n}_{H_2} HHV_{H_2} \quad (6)$$

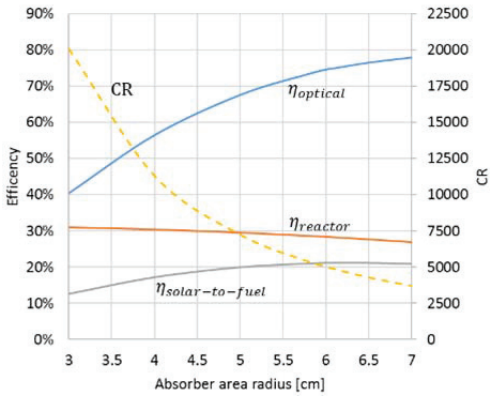

(a)

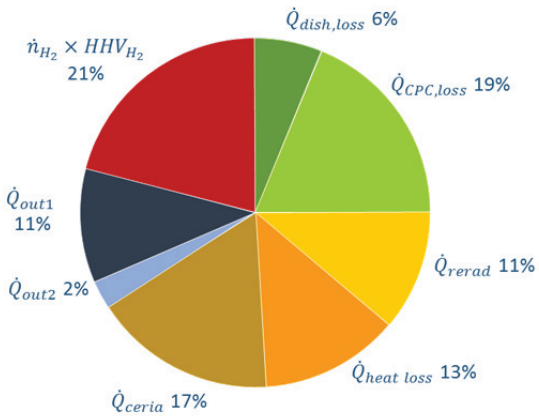

(b)

FIGURE 5: (a) Solar-to-fuel, optical and reactor efficiencies as a function of *r* and (b) overall system power balance for the 6 cm absorber radius case.

It is possible to notice that about 25% of the total solar input ($\dot{Q}_{sun} = 56.7\ kW$) is lost due to the system optical losses ($\dot{Q}_{dish,loss} + \dot{Q}_{CPC,loss}$), another 24% is related to system thermal losses (radiative and convective losses) and another 30% of losses is related to the heat required to heat up cerium oxide from the oxidation to the reduction temperature ($\dot{Q}_{ceria}$) and to the sensible heat of the two streams exiting the system. The last two contributions are computed taking into account the enthalpy (h) variation with respect to the reference state at T=T_0 and considering water at the liquid state.

$$\dot{Q}_{out1} = \dot{n}_{out1} \int_{T_0}^{T_{out1}} dh \qquad \dot{Q}_{out2} = \dot{n}_{out2} \int_{T_0}^{T_{out2}} dh \qquad (7)\ (8)$$

The higher value of $\dot{Q}_{out2}$ is due to the enthalpy of condensation of the steam contained in the flow exiting HEX_{ox}.

The loss related to the cerium oxide heating can be reduced as shown in Figure 6 if an active solid-phase recovery system were implemented [14], but, as suggested in [15], this would increase system complexity and thus it was not considered for the yearly analysis.

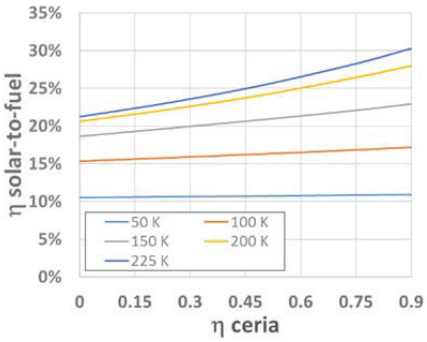

FIGURE 6: Impact of the variation of the cerium heat recovery efficiency η_{ceria} on the solar-to-fuel efficiency

RESULTS

In order to evaluate the yearly reactor performance, it was necessary to define the thermal losses variation as function of the operating conditions, namely DNI. Since reactor maximum temperature was kept constant for every operating condition (T_{red}= $T_{red,MAX}$), radiation and convection losses were assumed for simplicity just function of the maximum temperature and were thus assumed constant as well. The range of DNI analyzed goes from 325 W/m^2 (minimum operating radiation) to 1000 W/m^2. The variation of solar-to-fuel efficiency is reported in Figure 7.

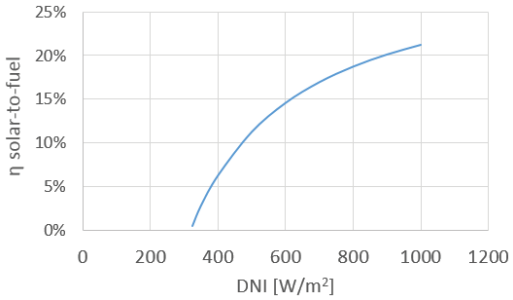

FIGURE 7: Solar-to-fuel efficiency of the Dish + Thermochemical reactor system as function of the solar radiation.

The off-design performance and the costs of the dish/Stirling system and of the PV system were computed within SAM, while the electrolyzer performance and cost were taken from [20]; elecrolyzer performance as function of the electric load can be considered with good approximation constant, while electrolyzer cost is assumed equal to 930 €/kW. The performances of the three considered solar driven technologies were analyzed and compared for two locations: Sevilla and Las Vegas. For the PV system the overall efficiency was defined with respect to the global radiation on the PV panels $G_{tot,\theta}$ defined as:

$$G_{tot,\theta} = DNI \times cos\theta + G_{diff,H} \times \frac{1 + cos\beta}{2} \qquad (9)$$

where $G_{diff,H}$ is the diffuse radiation on the horizontal plane and θ and β are the incidence and tilt angles of the panel respectively. Results are reported in Table 4.

TABLE 4. Yearly performance and economic analysis of the different considered systems

	Sevilla			Las Vegas		
	ThCh Reactor	**PV system**	**Dish / Stirling**	**ThCh Reactor**	**PV system**	**Dish / Stirling**
Nominal solar-to-fuel efficiency (%)	21.2	11.50	14.40	21.2	11.50	14.40
Annual Solar Energy (MWh_{th}/year)	100.59	117.27	100.59	147.78	137.76	147.78
Yearly Hydrogen yield (kgH_2/year)	358.50	285.155	282.43	623.07	335.70	434.97
Equivalent Hours (h_{eq})	1183	1255	1535	2056	1477	2363
Yearly solar-to-fuel efficiency (%)	14.15	9.65	11.15	16.72	9.67	11.68
Parabolic Dish cost (k€)	21.17	-	21.17	21.17	-	21.17
Stirling engine (k€)	-	-	7.92	-	-	8.15
PV system cost (k€)	-	17.90	-	-	17.90	-
Electrolyzer cost (k€)	-	7.50	8.05	-	8.38	9.48
LCOH (€/kWh_{H2})		0.324	0.494		0.294	0.335
ThCh reactor cost to match PV LCOH (k€)	9.72	-	-	27.6	-	-
ThCh reactor cost to match Stirling LCOH (k€)	25.9	-	-	34.4	-	-

Results highlight that although the solar-thermochemical system suffers of stronger performance decay at part-load operation, its higher nominal efficiency guarantees better results also on yearly basis. The yearly simulation showed for Las Vegas, the site with the highest radiation, a yearly solar-to-fuel efficiency of the solar-thermochemical system of 16.7%, corresponding to a hydrogen yield YHY of 623 kg_{H2}/y, which is higher than PV and dish/Stirling cases by about 85% and 43%, respectively. The preliminary economic analyses showed for the PV and the Dish/Stirling cases LCOH of about 0.294 and 0.335 €/kWh_{H2} respectively: the proposed system total investment cost to match the abovementioned LCOHs can thus be 1.85 and 1.43 times higher respectively. In Figure 8, the hourly hydrogen productivity (in kW) for the different considered systems is reported for a summer and a winter day.

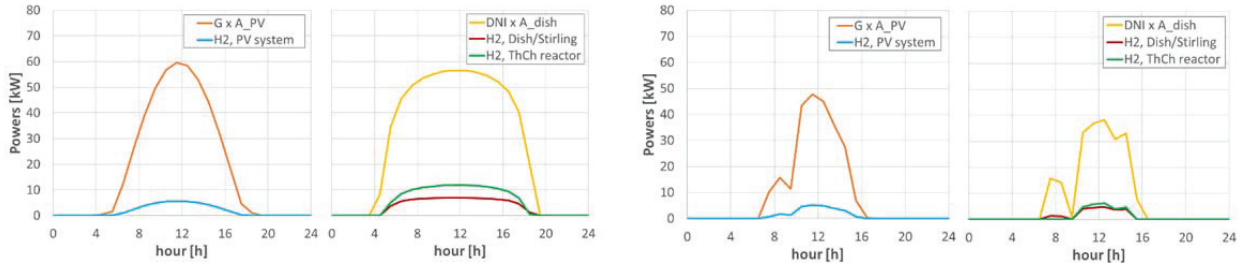

FIGURE 8: Global solar power ($G_{tot,\theta} \times A_{PV}$) on the PV panels, direct solar power hitting the solar dish (DNI × A_{dish}) and hydrogen production (in kW) for the different systems (a) on the 21st of June and (b) on the 22nd of December for Las Vegas.

During the summer day it is possible to notice how the tracking dish system allows for higher solar energy harvest with respect to the fixed PV panels, in particular around solar noon. It is also possible to notice how the hydrogen production of the solar-thermochemical system is higher during high DNI hours, but lower for very low DNI (e.g. at 8 a.m on the 22nd of December). The operating range of the solar-thermochemical system can be extended by reducing the design DNI.

CONCLUSIONS

In the present work the nominal and yearly performances of a solar driven thermochemical cycle were assessed. The optical model of a 56.7 m^2 parabolic dish used to collect the solar radiation coupled with a secondary CPC reflector used to rise the CR was developed in SolTrace. The reactor, based on nonstoichiometric cerium oxides thermochemical cycle, was modeled in Excel according to [15]. The two models were coupled and the concentration ratio was optimized in order to maximize the solar-to-fuel efficiency. For an isobaric reactor working with reduction/ oxidation temperatures of 1500°C/1275°C and no cerium heat recovery the maximum nominal solar-to-

fuel efficiency of 21.2% was achieved for an absorber radius of 6 cm, corresponding to a CR of about 5000. The hydrogen production as function of the DNI was estimated with the developed models assuming constant thermal losses; finally, with an hourly based simulation, a yearly solar-to-hydrogen efficiency of 16.72% was obtained for Las Vegas.

Two commercially available alternative technologies for the production of hydrogen with solar energy were also investigated: a PV system coupled with an electrolyzer and a Dish Stirling coupled with an electrolyzer. The two systems were designed assuming the same aperture area of the solar driven thermochemical system. For Las Vegas, the yearly solar-to-fuel efficiency of the PV system was 9.67%, while for the Dish/Stirling 11.68%.

The Levelized Cost of produced Hydrogen (LCOH) was computed for the two alternative systems and the investment cost of the thermochemical reactor was chosen in order to match the same LCOH. The PV and the Dish/Stirling estimated LCOHs for Las Vegas were of 0.294 and 0.335 €/kWh$_{H2}$ respectively: the proposed solar driven thermochemical system total investment cost to match the abovementioned LCOHs can thus be 1.85 and 1.43 times higher respectively.

REFERENCES

[1] FCH-JU, Study on hydrogen from renewable resources in the EU. Final report., (2015).

[2] J.E. Funk, Thermochemical hydrogen production : past and present, 26 (2001) 185–190.

[3] R. Perret, Solar Thermochemical Hydrogen Production Research (STCH) Thermochemical Cycle Selection and Investment Priority, Sandia Rep. (2011) 1–117.

[4] G.P. Smestad, A. Steinfeld, Review: Photochemical and thermochemical production of solar fuels from H2O and CO2 using metal oxide catalysts, Ind. Eng. Chem. Res. 51 (2012) 11828–11840. doi:10.1021/ie3007962.

[5] D. Thomey, L. de Oliveira, J.-P. Säck, M. Roeb, C. Sattler, Development and test of a solar reactor for decomposition of sulphuric acid in thermochemical hydrogen production, Int. J. Hydrogen Energy. 37 (2012) 16615–16622. doi:10.1016/j.ijhydene.2012.02.136.

[6] C. Huang, A. T-Raissi, Analysis of sulfur–iodine thermochemical cycle for solar hydrogen production. Part I: decomposition of sulfuric acid, Sol. Energy. 78 (2005) 632–646. doi:10.1016/j.solener.2004.01.007.

[7] A.K. Singh, N.J. Auyeung, K. Randhir, R. Mishra, K.M. Allen, J. Petrasch, et al., Thermal Reduction of Iron Oxide under Reduced Pressure and Implications on Thermal Conversion E ffi ciency for Solar Thermochemical Fuel Production, (2015). doi:10.1021/ie504402x.

[8] M.E. Galvez, P.G. Loutzenhiser, I. Hischier, A. Steinfeld, CO2 splitting via two-step Solar Thermochemical Cycles with Zn/ZnO and FeO/Fe3O4 Redox Reactions : Thermodynamic Analysis, Energy and Fuels. (2008) 3544–3550.

[9] R.B. Diver, J.E. Miller, M.D. Allendorf, N.P. Siegel, R.E. Hogan, Solar Thermochemical Water-Splitting Ferrite-Cycle Heat Engines, 130 (2015) 1–8. doi:10.1115/1.2969781.

[10] S. Abanades, P. Charvin, G. Flamant, Design and simulation of a solar chemical reactor for the thermal reduction of metal oxides: Case study of zinc oxide dissociation, Chem. Eng. Sci. 62 (2007) 6323–6333. doi:10.1016/j.ces.2007.07.042.

[11] C. Perkins, A.W. Weimer, Likely near-term solar-thermal water splitting technologies, 29 (2004) 1587–1599. doi:10.1016/j.ijhydene.2004.02.019.

[12] W.C. Chueh, S.M. Haile, A thermochemical study of ceria: exploiting an old material for new modes of energy conversion and CO2 mitigation, Philos. Trans. R. Soc. A Math. Phys. Eng. Sci. 368 (2010) 3269–3294. doi:10.1098/rsta.2010.0114.

[13] P. Furler, J. Sche, M. Gorbar, L. Moes, U. Vogt, A. Steinfeld, Solar Thermochemical CO 2 Splitting Utilizing a Reticulated Porous Ceria Redox System, (2012).

[14] D. Yadav, R. Banerjee, A review of solar thermochemical processes, Renew. Sustain. Energy Rev. 54 (2016) 497–532. doi:10.1016/j.rser.2015.10.026.

[15] R. Bader, L.J. Venstrom, J.H. Davidson, W. Lipiński, Thermodynamic analysis of isothermal redox cycling of ceria for solar fuel production, Energy and Fuels. 27 (2013) 5533–5544. doi:10.1021/ef400132d.

[16] T. Wendelin, A. Dobos, A. Lewandowski, T. Wendelin, A. Dobos, SolTrace : A Ray-Tracing Code for Complex Solar Optical Systems SolTrace : A Ray-Tracing Code for Complex Solar Optical Systems, (2013).

[17] T. Mancini, P. Heller, B. Butler, B. Osborn, W. Schiel, V. Goldberg, et al., Dish-Stirling Systems: An Overview of Development and Status, J. Sol. Energy Eng. 125 (2003) 135. doi:10.1115/1.1562634.

[18] L. Electronics, Mono X Black LG265S1K-A3, 2011.

[19] N. Blair, A.P. Dobos, J. Freeman, T. Neises, M. Wagner, T. Ferguson, et al., System Advisor Model , SAM 2014 . 1 . 14 : General Description, (2014).
[20] L. Bertuccioli, A. Chan, D. Hart, F. Lehner, B. Madden, E. Standen, Study on development of water electrolysis in the EU, (2014).
[21] W. Short, D.J. Packey, T. Holt, A Manual for the Economic Evaluation of Energy Efficiency and Renewable Energy Technologies, (1995) 462–5173.
[22] R.J. Panlener, R.N. Blumenthal, J.E. Garnier, A thermodynamic study of nonstoichiometric cerium dioxide, J. Phys. Chem. Solids. 36 (1975) 1213–1222. doi:10.1016/0022-3697(75)90192-4.
[23] M. Ricken, J. Nijlting, I. Riess, Specific Heat and Phase Diagram of Nonstoichiometric Ceria (CeO2-x), J. Solid State Chem. 54 (1984) 89–99.
[24] TUdelft, Refprop, (n.d.).
[25] I. Riess, M. Ricken, J. No¨lting, On the specific heat of nonstoichiometric ceria, J. Solid State Chem. 57 (1985) 314–322. doi:10.1016/0022-4596(85)90193-8.